Asian Journal of Chemistry; Vol. 31, No. 8 (2019), 1693-1703

ASIAN JOURNAL OF CHEMISTRY

https://doi.org/10.14233/ajchem.2019.21931

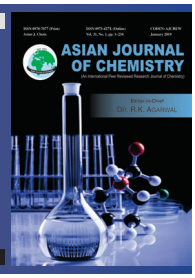

Experimental and DFT Study of Reaction Mechanisms in Removal of H_2S in Ferrites

E. AQUINO-TORRES[1], F. PRIETO-GARCÍA[2,*], J. PRIETO-MÉNDEZ[1], O.A. ACEVEDO-SANDOVAL[2] and R.A. CANALES-FLORES[2]

[1]Área Académica de Ciencias Agrícolas y Forestales, Universidad Autónoma del Estado de Hidalgo, Rancho Universitario, Tulancingo de Bravo,-Hidalgo, México
[2]Área Académica de Química, Universidad Autónoma del Estado de Hidalgo, Unidad Universitaria, km 4.5 Carretera Pachuca-Tulancingo, C.P. 42184 Pachuca-Hidalgo, México

*Corresponding author: E-mial: prietog@uaeh.edu.mx

Received: 10 January 2019; *Accepted*: 13 March 2019; *Published online*: 28 June 2019; AJC-19438

The objectives of this work were to synthesize and characterize manganese ferrites *via* hydrochemistry under optimized conditions to evaluate the adsorption capacity and removal of H_2S; calculation of the structural and electronic parameters involved in the process of adsorption between H_2S and Fe_3O_4 surfaces as majority phase ferrites in manganese and discern the process of physisorption or chemisorption. Relating experimental and theoretical on the mechanism of adsorption data allow us to conclude the interaction of H_2S with Fe_3O_4 and ferrites of manganese. The XRD patterns showed the majority of ferrites obtained magnetite phase. The adsorption capacity of H_2S on Mn ferrites indicate that the adsorption depends on the amount of iron and temperature. The XRD patterns after adsorption of H_2S show two corresponding to crystalline phases Fe_3O_4 and FeS_2 orthorhombic. Estimates of the volume of magnetite surfaces and adsorption of H_2S with Fe_3O_4 (111) with CRYSTAL09 code using the PBE0 functional and the data bases were performed using a modification of an iron base that improves the results of volume and surface adsorption H_2S on Fe_3O_4 (111) in FeO-Fet termination. BSSE results in the calculation of the energy of adsorption of H_2S were bridged site -17.50 kcal/mol base using Fe(III), -12.51 kcal/mol using the Fe(III) and Fe(II) bases simultaneously and -4.99 kcal/mol with the modified base. The energy of chemisorption process on octahedral iron was -48.42 kcal/mol, where the rupture of the -SH bond in the molecule and the formation of H_2S and O-H bond occurs at the surface. The experimental and theoretical evidence suggests that the adsorption capacity of the ferrites is limited to 50 %, as is the majority magnetite phase and it has two ends Fe_o-Fe_t and Fe_t-O energetically favoured. However, the former is reacted with hydrogen sulfide.

Keywords: Ferrites, Hydrogen sulfide, Chemisorption, Adsorption energy, CRYSTAL09.

INTRODUCTION

The removal treatment of H_2S depend largely on the medium in which it is present, in liquid or gaseous phase. They can be of four types: chemical, physical, biological or the combination of these [1,2]. To select the gas phase H_2S removal treatment, several factors must be taken into account, such as the composition of the gas as well as the amount of total sulfur, if the adsorbent is selective to H_2S. Another consideration is to know what the final disposal of the gas is, if it is desired to recover or only comply with the environmental rules and finally, the material costs. Another process in the gas phase is the adsorption consisting of passing the gases containing H_2S through a bed of solid adsorbent. Often this solid is recovered and the concentrated gas can be recovered, dried and reprocessed and the adsorbent is recycled [3-5]. Various investigations have shown that activated carbon impregnated with alkaline additives or oxides has higher efficiency and faster reaction kinetics compared to unmodified or virgin activated carbon [3,6-8].

At the end of the seventies, computational chemistry based on mathematical models for the prediction of chemical and physical properties of compounds searched. It is an area complementary to the experimental one, since it allows to obtain results that help the elucidation of a reaction mechanism supporting the observation, it allows to simulate an experiment with very reactive compounds that can be dangerous in the laboratory.

The Crystal09 program calculates the electronic structure of periodic systems with HF, density functional or hybrid

approaches. The block functions of periodic systems are expanded as linear combinations defined in terms of local functions (atomic orbitals) which in turn are linear combinations of Gaussian functions. The code can be used to perform studies of physical and chemical properties of molecules, polymers, surfaces and crystalline solids such as structural, vibrational properties, electronic structure, magnetic properties, *etc*. Closed-loop or polarized spin calculations can be carried out with all electrons and bases containing only the effective valence and pseudo potentional electrons. The pseudo potentials eliminate the internal electrons of the atom and represent them as a pseudo potential and the valence electrons keep moving in the potential generated by the nucleus and the internal electrons.

The oxides have been studied with the crystal code, particularly alkaline metals [2,9], TiO_2 in the anatase phase [10-12], as well as vacancies of oxygens in oxide crystals such as $SrTiO_3$ [13]. Recently, the crystal code has been used to search for materials that can be useful in spintronics, this has led to the study of ferromagnetic and antiferromagnetic materials [14]. Other iron-containing compounds such as goethite and lepidocrocite have been studied for their magnetic properties [15] and the compounds that are eventually found in nature such as the iron-containing olivine system [16].

Magnetite is a mixed oxide of iron ($FeO{\cdot}Fe_2O_3$) particular for its properties and structure. The volume and surfaces of the magnetite were studied with periodic calculations HF using CRYSTAL and pseudopotentials in 1999 [17], Patterson *et al.* [18] conducted a detailed study of magnetite and confirmed the orbital order and charge pattern based on NMR. In this work, the stability of the terminations in plane 111 is discussed, emphasizing that the most stable terminations are those that expose one or two layers of iron, since they preserve most of the coordinations of the surface atoms, besides the stability depends on stoichiometry and the dipole moment of the surface. The surface with sequence Fe_2O_4, Fe_3O_4, Fe_2 is favoured because it ensures the neutrality of the dipole moment. On the other hand, this sequence, which is also symmetric, the iron atoms could present an excessive oxidation so they can be reduced by hydrogenation and gain stability.

In 2009, the volume of Fe_3O_4 with the functional hybrid B3LYP and a functional GGA PW91 using the CRYSTAL06 version and the iron base for Fe_2O_3, the results of the electronic behaviour of magnetite for these two functional elements were studied [18] are different, while the functional GGA shows the magnetite with a metallic character, B3LYP predicts a sorting of charges as semiconductor. This highlights the importance of the functional choice. Fe_3O_4 is found in nature, often as octahedral crystals and exhibits faces 111 and rarely as a dodecahedron with faces 001, for this reason in this study we worked with plane 111. The termination of surface 111 of Fe_3O_4 consists of ¼ of monolayer of Fe atoms in tetrahedral positions on an oxygen layer, this model has been proposed as the most stable termination [19-21].

There are few works of magnetite made with the code CRYSTAL and many made with other programs such as CASTEP and VASP that use a different methodology to include increased flat waves instead of atomic orbitals.

The BSSE base overlap error is attributable to the Roothaan method, because the base set used is not complete, the results of the calculations depend on the quality of the base, that is, very large bases to obtain good results. Close to the HF limit, this error tends to disappear as the quality of the bases used increases. The error is estimated by the counterweight method; in a system composed of A/B, the energy of the isolated fragment A (in its relaxed geometry) is evaluated considering the base set of B and vice versa; in CRYSTAL the BSSE calculations are easily performed.

The objective of the work was to synthesize and characterize Mn ferrites by hydrochemical method under optimized conditions to evaluate the capacity of H_2S adsorption. The calculation of the structural and electronic parameters involved in the adsorption process between the H_2S and Fe_3O_4 surfaces as the majority phase in the Mn ferrites, to discern the physisorption or chemisorption process. To relate the experimental and theoretical data about the mechanism of adsorption, which allow to conclude the interaction of H_2S with Fe_3O_4 and Mn ferrites.

EXPERIMENTAL

The synthesis of Mn ferrites was performed under parameters reported as optimal obtained in previous works [22,23]. To obtain the ferrites, solutions were prepared using $Mn(NO_3)_2{\cdot}6H_2O$ in a concentration of 1000 ppm of the Mn(II) ion.

In a 500 mL reactor [23] connected to a thermostat, 300 mL of the $Mn(NO_3)_2{\cdot}6H_2O$ solution was added, a combined electrode (glass-Calomell) and a temperature sensor were introduced. The solution was stirred and maintained at 60 °C, then 22.40 g of $FeSO_4{\cdot}7H_2O$ were added, after its dissolution, a few drops of 2 M NaOH solution were added and a flow of air was contacted, the Basic solution until the pH is adjusted to 10 ± 0.2 for 1 h. After the reaction time elapsed, the solution was allowed to cool to room temperature and filtered under vacuum. The clear liquid was reserved for analysis of the remaining concentration of Mn^{2+}, the solid was washed with large amount of distilled water to eliminate excesses of NaOH and Na_2SO_4. Later it was dried at 105 °C in an oven for 2 h. The purified water was neutralized with HCl to a pH between 6-7.5; being ready for dumping. Syntheses were made with air flows of 0.7, 0.5 and 0.3 L/min.

The ferrites obtained were characterized 0.1 g was weighed, dissolved in 5 mL of HNO_3 and diluted to 50 mL. 5 mL were taken and 100 mL were analyzed to be analyzed by atomic emission spectroscopy with inductively coupled plasma (ICP). For the analysis, a Perkin Elmer Optima 3000 spectrophotometer was used. The concentration of Mn(II) and total Fe was determined. The determination of Fe(II) was carried out by the photocolorimetric method of *o*-phenanthroline by UV-visible spectrophotometry in a Perkin Elmer Instruments Lambda 40 UV/visible spectrometer. Fe(II) standards were prepared in a concentration of 0.0 to 0.5 mg, ammonium acetate/acetic acid buffer solution (pH = 4.2) [22].

The diffractograms were obtained from a PHILIPS diffractometer, model PW-1710-BASED, with CuKα radiation source, $\lambda = 0.154$ nm, nickel filter, aluminum sample holder, generator voltage and current of 40 KV and 30 mA, respectively with sweeps of angles (2θ) from 5 to 70 [22].

To study the H_2S adsorption capacity of manganese ferrites, 9 experiments were carried out with three replications, at 100, 125 and 150 °C. 1 g of manganese ferrite, previously dried for 2 h at 105 °C, was weighed and placed in a fixed bed reactor of 27 cm long and 1 cm in diameter, which was placed in a furnace to keep the temperature constant by means of a controller (Fig. 1). The gas was supplied from a tank at 10 % H_2S/H_2. A flow of 40 cm^3/min equivalent to a concentration of 0.0053 M H_2S and a time of 60 min was passed.

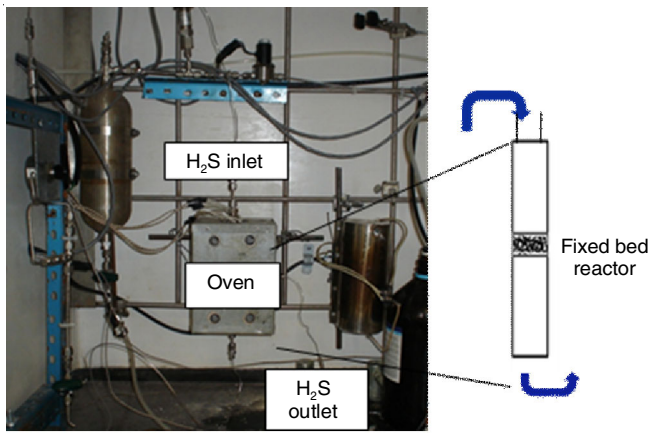

Fig. 1. Equipment for adsorption

All the experiments were performed at atmospheric pressure and the quantification of H_2S was done by samples taken every 10 min, bubbling H_2S/H_2 mixture in I_3^- solution of known concentration for 15 s, at the exit of the reactor. At the end of the experiment the reactor was weighed with ferrite and by weight difference the adsorbed H_2S was calculated. The solution of I_3^- was prepared according to Pisani *et al.* [24] as well Aquino and Prieto [25]. The adsorption capacity was obtained with the following expression:

$$\text{Adsorption capacity (\%)} = \frac{\text{Adsorbed mass of } H_2S}{\text{Ferrite mass}} \times 100 \quad (1)$$

All calculations were made with the code *ab initio* CRYSTAL09. This code implements Hartree-Fock and self-consistent Kohn-Sham field methods for the study of periodic systems [22]. The functional PBE0 was used, which has good results in studies of structural and electronic properties [26] of TiO_2. The available iron bases were used: Fe(III) [27] used for hematite and Fe(II) [28] optimized for FeF_2 and a base that was modified from the base of Faith (II). For O the base used in NiO was taken [27] and for S and H the bases 6-311 ++ G** [29]. For the integration of the Brillouin area, the Monkhorst-Pack (6'6'6) and (8'8'8) schemes were used to calculate the DOS state density. A truncation tolerance was considered for the bielectronic integrals of 7 7 7 7 14 used for the study of magnetite volume [30]. For all calculations, the convergence criterion of the SCF was 10-7. The volume of magnetite was cut in the plane (111) and the possible surface terminations were studied: Fe_t-O tetrahedral iron-oxygen, O-Fe_t tetrahedral iron-oxygen, Fe_o-Fe_t octahedral iron-tetrahedral iron, Fe_t-Fe_o tetrahedral iron-octahedral iron, O-O-iron octahedral-oxygen and O-Fe_o oxygen-octahedral iron; which were modeled with 10 layers formed by two units of Fe_3O_4. The calculations of the surfaces were made with the same parameters as the volume and the atomic charges were calculated with the Mulliken method. For the adsorption of H_2S it was done on the Fe_o-Fe_t surface at the bridging site and on the Urea with the plane of the molecule horizontal to the surface. The adsorption energy is given by the equation:

$$E_{ads} = E_{sdup-H_2S} - (E_{sup} + E_{H_2S}) \quad (2)$$

where $E_{sup\text{-}H_2S}$ is the total energy of the surface and H_2S, E_{sup} is the energy of the clean surface and E_{H_2S} the energy of H_2S isolated.

RESULTS AND DISCUSSION

Table-1 shows the results of the Mn ferrites obtained with three different air flows. It can be seen that there are no significant differences in the percentage of Mn(II) incorporated, percentage of total Fe and in the stoichiometries obtained at the different air flows; however, a small decrease in Fe(II) content is observed with the increase in air flow.

Fig. 2 shows the XRD ferrite patterns of Mn varying the air flow, in which the majority magnetite phase is observed, counting eight peaks corresponding to this oxide. Table-2 summarizes the experiments carried out in triplicate with ferrites of Mn and magnetite. All H_2S adsorbed mass values are lower compared to $CaFe_2O_3$ calcium ferrites prepared with activated carbon that adsorb almost 100 % of their reported stoichiometry [31].

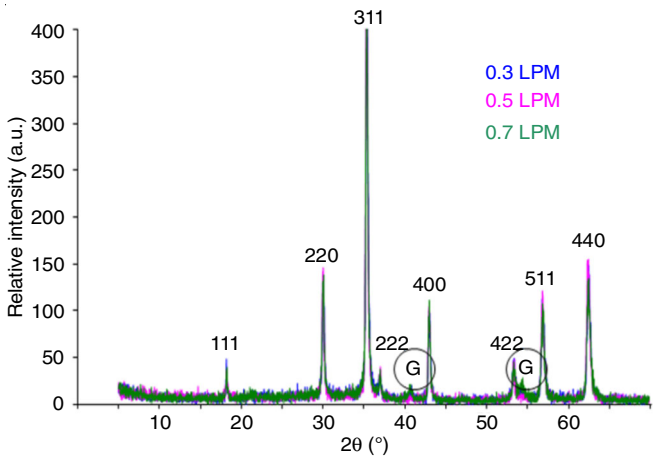

Fig. 2. Diffractograms of Mn ferrites to three air flows. G indicates presence of goethite

TABLE-1
METAL CONTENT AND STOICHIOMETRY OF Mn FERRITES USING THREE DIFFERENT AIR FLOWS. IN PARENTHESES THE STANDARD DEVIATION

Air flow (L/min)	% Metal (m/m)	% m/m Fe(II)	% m/m Fe_{total}	% m/m Fe(III)	Fraction Mn(II)	Formula
0.3	12.09 (0.000)	20.33 (0.010)	68.81 (0.129)	48.48 (0.189)	0.12	$Mn_{0.12}Fe_{2.88}O_4$
0.5	11.85 (0.000)	19.46 (0.117)	68.36 (0.095)	48.90 (0.085)	0.12	$Mn_{0.12}Fe_{2.88}O_4$
0.7	11.85 (0.000)	19.08 (2.264)	68.77 (0.213)	49.69 (0.213)	0.12	$Mn_{0.12}Fe_{2.88}O_4$

TABLE-2
ADSORBED MASS OF H_2S IN FERRITES OF Mn AND Fe (MAGNETITE). FIXED EXPERIMENTAL CONDITIONS: TIME 60 min, H_2S CONCENTRATION 0.0053 M

Metallic ferrite	Adsorption temperature (°C)	Adsorbed mass of H_2S (mg)	Adsorption capacity per g of ferrite (%)
Mn	100	96.5	23.6
Mn	125	111.0	27.1
Mn	150	123.0	30.1
Fe	100	109.8	26.8
Fe	125	117.2	28.7
Fe	150	133.4	32.6

This may be due to the fact that activated carbon is considered one of the best adsorbents for gases [32] and when mixed with ferrites it improves the adsorption capacity. The evaluation of the removal capacity of Mn ferrites at 100, 125 and 150 °C, with 1 g of solid, a contact time of 60 min and an H_2S concentration of 0.0053 M was proposed. The results show that the adsorption of H_2S is favoured when the temperature increases.

This suggests that the adsorption is a function of the amount of iron present, if we analyze the composition of the ferrite of Mn, for each ion of Mn(II) there are 24 Fe ions, of which 7 are Fe(II) and remaining are Fe(III) explains that it has less adsorption than magnetite. Fig. 3 shows the XRD patterns for Mn ferrite after the adsorption of H_2S, we observe the majority phase magnetite when counting 8 peaks, it is difficult to see a peak corresponding to FeS_2 (marcasite). This is because Mn ferrite has a low capacity of H_2S adsorption at the evaluated temperatures.

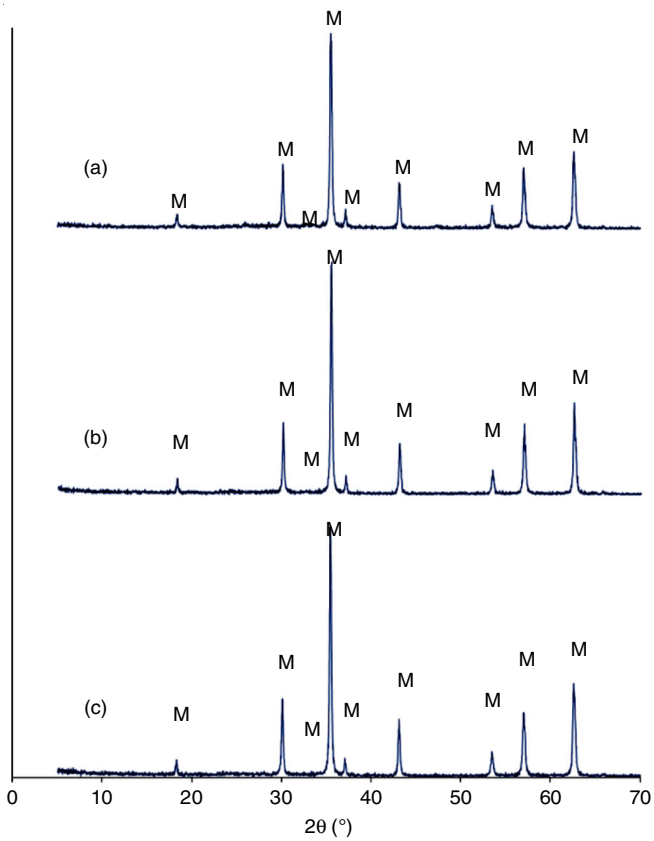

Fig. 3. XRD patterns of $Mn_{0.12}Fe_{2.88}O_4$ after adsorption (a) 100, (b) 125 and (c) 150 °C. Legends: Fe_3O_4 (M), FeS_2 type marcasite (Ma)

The optimization of the volume structure was carried out with the functional PBE0 and the Fe(III) base of Catti *et al.* [27], to represent the Fe(II) and Fe(III) ions in the magnetite. In the volume there are two types of octahedral-oxygen iron bond (Fe_o-O) which are Fe1-O, Fe2-O, Fe3-O and Fe4-O and tetrahedral-oxygen iron bonds (Fe_t-O) corresponding to Fe5-O and Fe6-O, these distances are presented in Table-3 and are consistent with the experimental distances Fe_o-O of 2.07 Å and Fe_t-O of 1.88 Å [32-34].

TABLE-3
Fe–O BOND DISTANCES IN Fe_3O_4 VOLUME

Bond	Distance (Å)	Bond	Distance (Å)
Fe1–O8	2.00	Fe3–O7	2.09
Fe1–O10	2.00	Fe3–O8	2.09
Fe1–O11	2.04	Fe3–O12	2.14
Fe1–O12	2.04	Fe4–O7	2.09
Fe1–O13	2.04	Fe4–O8	2.09
Fe1–O14	2.04	Fe4–O11	2.14
Fe2–O7	2.00	Fe5–O7	1.88
Fe2–O11	2.04	Fe6–O9	1.88
Fe2–O12	2.04	–	–

The electronic properties (charges, magnetic moments and density of states) of the volume allow to analyze the chemical reactivity of atoms. The magnetic charges and magnetic moments in the volume are presented in Table-4. The charges of the irons in octahedral sites (Fe_o) approximate the formal charge reported, four Fe in octahedral sites of which two must have a charge of 3+ and the remaining of 2+, while the Fe in tetrahedral position must have a charge of 3+. The total magnetic moment per unit of Fe_3O_4 was 4 μB, according to the experimental 4.05 μB [32]. The results show a network parameter a = 8.43 Å, with angles $\alpha = \beta = \gamma = 90°$ and a coordination parameter x of the oxygen ion of 0.2521 (Fig. 4). These values are similar to those obtained experimentally 8.396 Å and x = 0.2549 [33] and with the reported calculations [30].

TABLE-4
CHARGES AND MAGNETIC MOMENTS OF IONS IN Fe_3O_4 VOLUME

Atom	Charges (u.a)	Magnetic moment (μ_B)
Fe1	2.24	4.33
Fe2	2.24	4.33
Fe3	1.84	3.76
Fe4	1.84	3.76
Fe5	2.17	–4.24
Fe6	2.17	–4.24
O7	–1.56	0.00
O8	–1.56	0.00
O9	–1.57	0.07
O10	–1.57	0.08
O11	–1.56	0.00
O12	–1.56	0.00
O13	–1.57	0.08
O14	–1.57	0.08

The density of states (DOS) shows the number of energy levels allowed in a range of energy dE [35,36]. Fig. 5 shows the density of magnetite volume states for sites A (tetrahedral irons), sites B (octahedral irons) and O sites (oxygens), where we can see a greater contribution of occupied and unemployed states

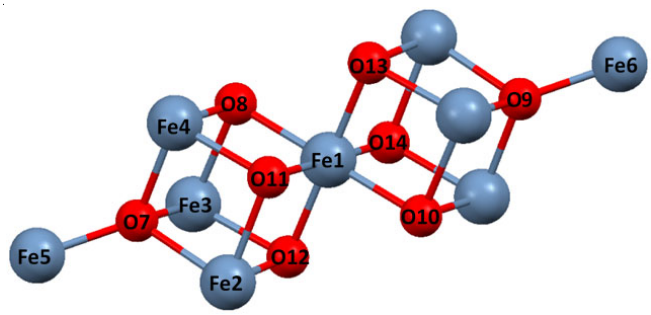

Fig. 4. Structure of Fe_3O_4 with 14 atoms: 6 iron ions (4 Fe^{3+} and 2 Fe^{2+}) and 8 oxygen ions (O_2^-)

of type *d* corresponding to Fe_o located at higher energy levels with respect to the tetrahedral irons, these levels are similar to those of Rowan *et al.* [18].

To obtain the magnetite surfaces the volume was cut in the plane (111), the six possible terminations are Fe_o-O, O-Fe_t, Fe_o-Fe_t, Fe_t-Fe_o, Fe_t-O and O-Fe_o. These surfaces were modeled with ten layers consisting of two Fe_3O_4 units fulfilling the stoichiometry of the magnetite formula unit and the charge neutrality. In addition, the total spin of the volume was taken for the calculation of all the surfaces; surfaces with optimized Fe_o-Fe_t and Fe_t-O terminations showed lower energies with respect to the other four terminations [37].

In this paper only the two most stable surfaces are described, the calculated energies were -5134583.72 and -5134587.67 kcal/mol for Fe_o-Fe_t and Fe_t-O respectively with an energy difference of 3.95 kcal/mol between them. The above suggests that these two surfaces are stable and that they can coexist according to the findings of Lennie *et al.* [38], who studied Fe_3O_4 (111) by means of Tunnel Effect Microscopy and distinguished two coexisting terminations, which have dimensions of the identical hexagonal unit cell (Figs. 6 and 7).

It is important to mention that to calculate the ferrimagnetic structure (with spin of 4 μB per unit of magnetite) we started from the optimized geometry of the ferromagnetic surfaces. Figs. 8 and 9 show the surfaces Fe_o-Fe_t and Fe_t-O with ferromagnetic arrangement (all the spins of the α-irons) and ferrimagnetic (with α and β spins in such a way that

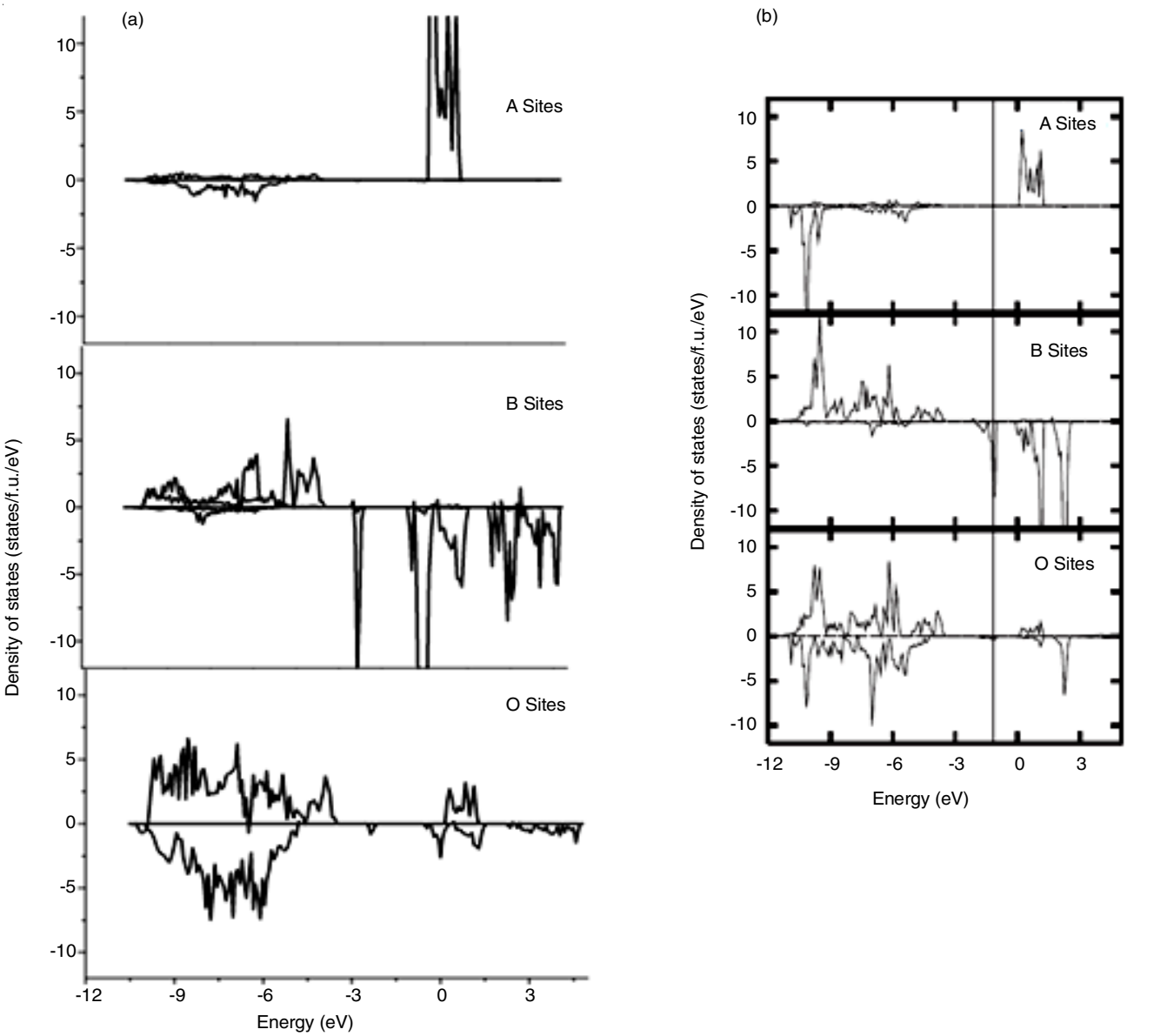

Fig. 5. DOS comparison of the Fe_3O_4 volume: (a) calculated with the functional PBE0 and (b) calculated with B3LYP by Rowan *et al.* [18]

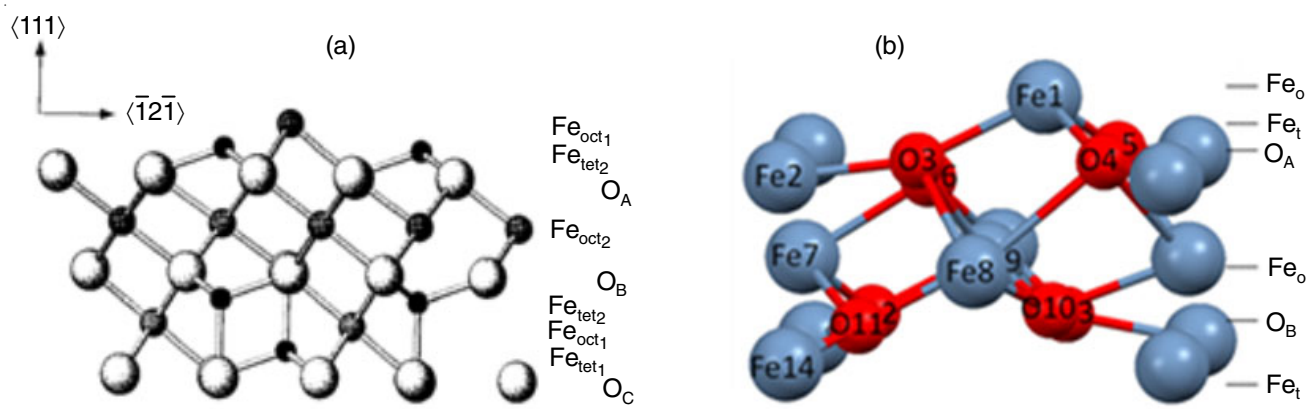

Fig. 6. Comparison of the Fe_o-Fe_t surfaces (a) surface observed by Lennie *et al.* [38] and (b) surface optimized in this work

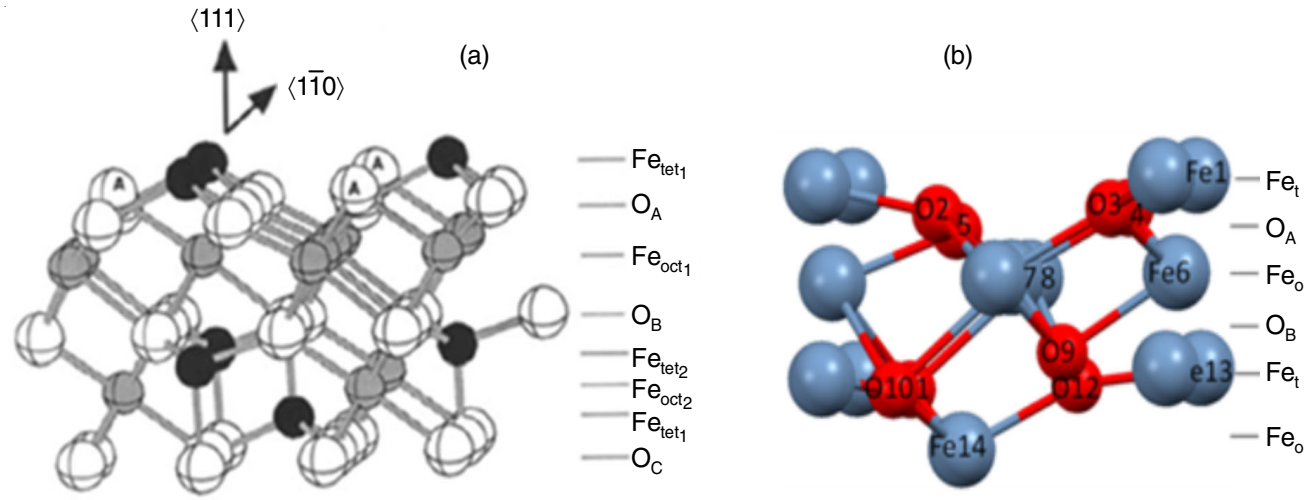

Fig. 7. Comparison of the surfaces Fe_t-O, (a) surface observed by Condon *et al.* [20] and (b) surface optimized in this work

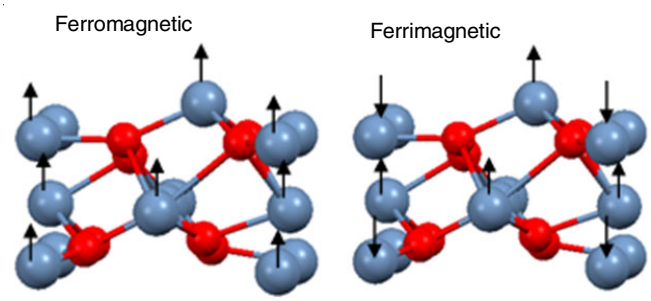

Fig. 8. Ferromagnetic and ferrimagnetic arrangement of the spins of the irons on the surface of Fe_3O_4 with Fe_o-Fe_t termination

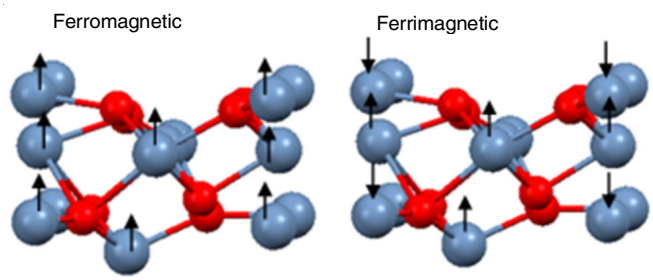

Fig. 9. Ferromagnetic and ferrimagnetic arrangement of the spins of the irons on the surface of Fe_3O_4 with Fe_t-O termination

the magnetic moment cannot be canceled, resulting in magnetic moment total of 4 μB).

Table-5 shows the calculated energies for the ferromagnetic and ferrimagnetic systems with different spin values for the Fe_o-Fe_t and Fe_t-O surfaces. For the Fe_o-Fe_t surface, the energy difference between the ferromagnetic system and the ferrimagnetic with spin of 4 μB was 5.86 kcal/mol, while for the Fe_t-O surface this difference was 1.87 kcal/mol suggesting that the ferromagnetic system is slightly more stable than the ferrimagnetic system with spin of 4 μB. On the other hand, when comparing the two systems of lower energy of both surfaces Fe_o-Fe_t and Fe_t-O, the ferromagnetic and ferrimagnetic of 5 μB show energy differences of 18.34 and 20.02 kcal/mol, respectively; *i.e.*, the ferrimagnetic surfaces (Fe_o-Fe_t and Fe_t-O) with total spin of 5 μB are the most stable.

TABLE-5
ENERGIES OF THE MOST STABLE SURFACES OF Fe_3O_4 (111) WITH SPINS IN FERROMAGNETIC AND FERRIMAGNETIC ARRANGEMENT

Surface	Energy (kcal/mol)
Fe_o–Fe_t (ferromagnetic with spin 14)	–5134589.58
Fe_o–Fe_t (ferrimagnetic with spin 4)	–5134583.72
Fe_o–Fe_t (ferrimagnetic with spin 5)	–5134608.04
Fe_t–O (ferromagnetic with spin 14)	–5134589.54
Fe_t–O (ferrimagnetic with spin 4)	–5134587.67
Fe_t–O (ferrimagnetic with spin 5)	–5134609.56

The charges and magnetic moments of the ions were calculated on the Fe_o-Fe_t and Fe_t-O surfaces with total magnetic moment of 5 μB for each unit of Fe_3O_4, the Fe_o and Fe_t exposed on the Fe_o-Fe_t and Fe_t-O surfaces, respectively and they have been labeled as Fe1 and we will continue to call them octahedral and tetrahedral according to the place they occupied in the volume.

Initially, the H_2S molecule was approached in a bridging site between Fe_o-Fe_t with the molecular plane parallel to the surface (Fig. 10) using the functional PBE0 and the iron base [25] to model Fe(II) and Fe(III) in magnetite. The results obtained for this approach are: link distances S-H 1.35 Å, Fe_o-S 3.89 Å and Fe_t-S 2.54 Å. The adsorption energy was calculated with the aforementioned eqn. 2, the results showed that the energy was -5385161.91 kcal/mol, E_{sup} -5134608.04 kcal/mol and E_{H_2S} -250537.33 kcal/mol, obtaining an adsorption energy of -16.54 kcal/mol.

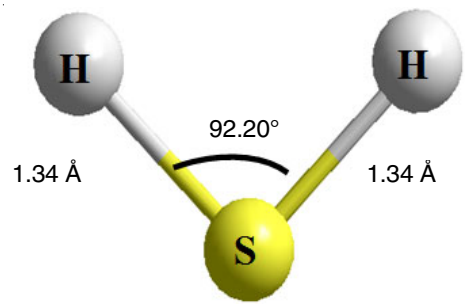

Fig. 10. Optimized H_2S structure, S-H bond distances and H-S-H bond angle

It is important to mention that when studying surface phenomena, the base superposition error BSSE must be calculated to obtain a corrected value of the adsorption energy. This error is attributable to the fact that the base set is generally not complete, the results of the calculations depend on the quality of the base, *i.e.*, very large bases are required to obtain results close to the limit of the exact energy. This error tends to disappear as the quality of the bases used increases. The error calculated for this adsorption was -17.50 kcal/mol, *i.e.*, the error caused by the base is greater than 100 % of the adsorption energy, so this result is unacceptable for modeling the adsorption of H_2S on magnetite. For example, in Table-6 it is observed that the octahedral iron Fe1 exposed to the outside of the Fe_o-Fe_t surface is in an oxidation state of approximately 2+ as well as the tetrahedral iron Fe14. It is also observed that in the Fet-O surface, tetrahedral iron Fe1 has an oxidation state close to 2+ as well as octahedral iron Fe14. It is also observed that in the Fe_t-O surface, tetrahedral iron Fe1 has an oxidation state close to 2+ as well as octahedral iron Fe14. This is because, like the spinel $MgAl_2O_4$; presents a termination with monolayers of Mg^{2+}; the stability of the endings of the magnetite surfaces depends on the cut generated by the surfaces, the smallest possible number of bonds must be broken and the surface atoms are cations in low oxidation state this together with the relaxation contributes to the reduction of the dipole moment perpendicular to the surface [17].

The structural and electronic properties of the isolated H_2S are important to perform the calculation of the adsorption energy and the analysis of the charge transfer. The energy calculated with PBE0 was -250537.33 kcal/mol; the S-H bond

TABLE-6
COMPARISON OF Fe–O BOND DISTANCES IN THE VOLUME OF Fe_3O_4 CALCULATED WITH THE BASE OF Fe(III) AND THE MODIFIED BASE

Bond	Bond distances (Å)	
	Base of Fe(III)	Modified base
Fe1–O8	2.00	2.02
Fe1–O10	2.00	2.02
Fe1–O11	2.04	2.05
Fe1–O12	2.04	2.05
Fe1–13	2.04	2.05
Fe1–14	2.04	2.05
Fe2–O7	2.00	2.02
Fe2–O11	2.04	2.05
Fe2–O12	2.04	2.05
Fe3–O7	2.09	2.09
Fe3–O8	2.09	2.09
Fe3–O12	2.14	2.13
Fe4–O7	2.09	2.09
Fe4–O8	2.09	2.09
Fe4–O11	2.14	2.13
Fe5–O7	1.88	1.88
Fe6–O9	1.88	1.88

distances are 1.34 Å and the H-S-H bond angle of 92.20° (Fig. 11). These values are in agreement with the experimentally reported; in addition, the charges obtained were -0.18 for the sulfur atom and 0.09 for the hydrogen atom.

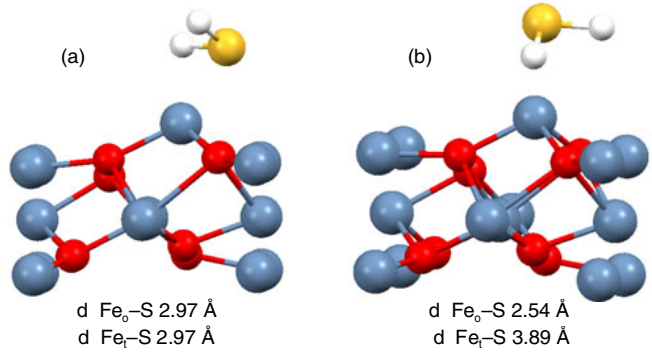

Fig. 11. Approximation of H_2S in the Fe_o-Fe_t bridge site, (a) before adsorption, (b) after adsorption

To solve the BSSE problem it was necessary to modify or implement a new iron base that allows to provide greater flexibility by increasing the number of layers of the *d* orbitals. Initially the Fe(III) base was used and a layer *d* was added and the exponents and coefficients were calculated, however, the computational cost was demanding without obtaining the expected results. Subsequently, the Fe(II) base was taken, to which a d layer was added and the exponents and coefficients were calculated successfully. Slight modifications were observed, the introduction of another *d* layer and the modification of the last line of the exponents and coefficients of the second *d* layer. When the base changes it is essential that calculations are made again from volume, since this change is important in the calculation of energy of the system. The geometrical parameters of the volume and magnetite surfaces were calculated without showing significant changes with those calculated previously: a network parameter of 8.44 Å, angles $\alpha = \beta = \gamma =$ 90 ° and an oxygen ion coordination parameter of 0.2521; Fe-O bond distances are shown in Table-6.

On the other hand, a comparison was made of the changes in energy of the volume and surfaces of Fe_3O_4 (111) when using the modified base and Fe(III) base. For the volume, an energy difference of 25.33 kcal/mol was obtained, while for the Fe_o-Fe_t and Fe_o-O surfaces they were 69.50 and 68.02 kcal/mol, respectively. These values indicate that the energies decrease when using the modified base (Table-7).

TABLE-7
DIFFERENCES IN ENERGY WHEN USING Fe(III) BASE AND THE MODIFIED BASE IN THE CALCULATION OF THE VOLUME AND SURFACES OF Fe_3O_4 (111)

Calculation	Energy with the base Fe(III) (kcal/mol)	Energy with the modified base (kcal/mol)	Energy difference (kcal/mol)
Volume	–5134764.46	–5134789.79	25.33
Surface Fe_o–Fe_t	–5134608.04	–5134677.55	69.50
Surface Fe_t–O	–5134609.56	–5134677.58	68.02

Table-8 shows the coordinates of the ions of the surface generated in the plane (111) with Fe_o-Fe_t termination before and after the optimization, likewise the interplanar distances that indicate the interatomic distance in the z axis that change when the ions relax and may increase or decrease. For example, the interplanar distance between Fe1-Fe2 (octahedral iron-tetrahedral iron) changes from 0.59 to 0.75 Å before and after the optimization respectively, while the position of Fe1 decreases from 2.14 to 1.79 Å in the z axis. Fig. 12 showed that the distance A and B of the cell increases from 5.97 to 6.16 Å while in C it decreases due to the relaxation of the ions mainly of the Fe1 and Fe2 atoms.

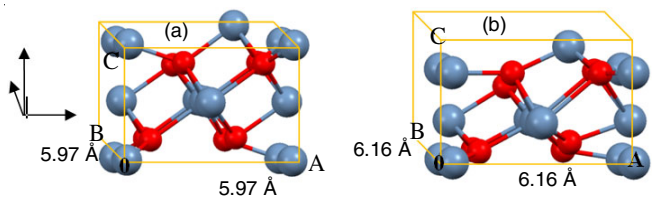

Fig. 12. Relaxation of the surface of Fe_3O_4 (111) Fe_t-O with respect to the atomic positions in the volume; (a) before and (b) after the optimization

Table-9 shows the interplanar distances before and after the optimization of the Fe_t-O surface; there is a decrease in the interplanar distance between Fe1-O2 (tetrahedral iron-

TABLE-8
COORDINATES OF THE IONS OF Fe_o–Fe_t SURFACE BEFORE AND AFTER THE OPTIMIZATION AND THE INTERPLANAR DISTANCES BEFORE AND AFTER THE OPTIMIZATION

Atom	Coordinates in the volume			Optimized coordinates			Interplanar distance (Å)	
	x	y	z	x	y	z	Before	After
Fe1	–2.81	1.83	2.14	–2.90	1.88	1.79	0.59	0.75
Fe2	0.21	0.12	1.56	0.19	0.11	1.04	0.60	0.03
O3	1.75	1.01	0.96	1.78	1.02	1.02	0.02	0.00
O4	–1.35	1.05	0.94	–1.40	1.03	1.02	0.00	0.00
O5	0.24	–1.69	0.94	0.18	–1.73	1.02	0.09	0.45
O6	3.11	–1.65	0.85	–2.90	–1.67	0.57	1.14	1.01
Fe7	1.67	–2.48	–0.29	–1.29	2.81	–0.44	0.00	0.01
Fe8	–2.81	0.10	–0.29	–2.90	0.03	–0.45	0.00	0.00
Fe9	–1.31	–2.48	–0.29	–1.42	–2.52	–0.45	1.14	0.62
O10	–2.75	1.86	–1.44	0.18	–3.45	–1.07	0.09	0.28
O11	0.12	1.90	–1.52	0.19	1.90	–1.35	0.00	0.00
O12	1.70	–0.85	–1.52	1.74	–0.79	–1.35	0.02	0.00
O13	–1.39	–0.80	–1.54	–1.37	–0.79	–1.36	0.60	0.29
Fe14	0.15	0.09	–2.14	0.18	0.11	–1.65	–	–

TABLE-9
COORDINATES OF THE IONS OF Fe_t–O SURFACE BEFORE AND AFTER THE OPTIMIZATION AND THE INTERPLANAR DISTANCE AFTER THE OPTIMIZATION

Atom	Coordinates in the volume			Optimized coordinates			Interplanar distance (Å)	
	x	y	z	x	y	z	Before	After
Fe1	–0.15	–0.09	2.14	–0.18	–0.11	1.65	0.60	0.30
O2	1.39	0.80	1.54	1.37	0.79	1.35	0.02	0.00
O3	–1.70	0.85	1.52	–1.73	0.79	1.35	0.00	0.00
O4	–0.12	–1.90	1.52	–0.19	–1.90	1.35	0.09	0.28
O5	2.75	–1.86	1.44	2.90	–1.89	1.07	1.14	0.62
Fe6	–1.67	2.48	0.29	1.29	–2.81	0.44	0.00	0.00
Fe7	2.81	–0.10	0.29	2.90	–0.03	0.45	0.00	–0.01
Fe8	1.31	2.48	0.29	1.42	2.52	0.45	1.14	1.03
O9	–3.11	1.65	–0.85	2.89	1.68	–0.57	0.09	0.45
O10	–0.24	1.69	–0.94	–0.18	1.73	–1.02	0.00	0.00
O11	1.35	–1.05	–0.94	1.40	–1.03	–1.02	0.02	0.00
O12	–1.75	–1.01	–0.96	–1.78	–1.02	–1.02	0.60	0.02
Fe13	–0.21	–0.12	–1.56	–0.18	–0.11	–1.04	0.59	0.75
Fe14	2.81	–1.83	–2.14	–0.18	3.45	–1.79	–	–

oxygen) from 0.60 to 0.30 Å and a relaxation of tetrahedral iron Fe1 changing from 2.14 to 1.65 Å before and after optimization, respectively, on the z axis of y (Fig. 13).

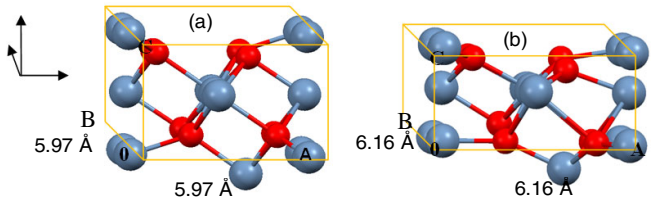

Fig. 13. Approximations of H_2S in the Fe_o-Fe_t bridge site; (a) before and (b) after adsorption

With this modified base, the adsorption on the Fe_o-Fe_t surface was carried out in two approximations at the bridging site between Fe_o-Fe_t and on Fe_o with the molecular plane parallel to the surface as shown in Fig. 13. In the approach at the bridge site, the distances between the atoms Fe1-S (octahedral iron-sulfur) and Fe2-S (tetrahedral iron-sulfur) were 3.89 and 2.54 Å, respectively. These values do not vary with respect to the base used previously and the modified one. However, the adsorption energy does change and was -12.70 kcal/mol with a BSSE of -4.99 kcal/mol. The value of BSSE represents 39 % of the adsorption energy which is acceptable for the purposes of this work.

The adsorption energy calculated for the in-bridge system was -7.70 kcal/mol, corresponding to a physisorption process characterized by weak adsorbate-adsorbent attractions.

On the other hand, the adsorption of H_2S on Fe_o with the molecular plane horizontal to the surface was also carried out since this atom loses three oxygen atoms that are eliminated when cutting the volume in the plane (111), so that the atom octahedral iron (Fe1) represents the ideal site for the adsorption of H_2S preferentially on Fe1 (Fe2) that loses only one oxygen atom when forming the surface.

The adsorption of H_2S on Fe_o showed a breakdown of S-H bond (Fig. 14); the bond distances Fe1-S and O-H were 2.33 and 1.04 Å, respectively. These results suggest the formation of Fe-S and O-H covalent bond corresponding to a chemisorption. The result was validated with the calculation of the link energy which was -48.42 kcal/mol. Fig. 15 allows proposing a possible mechanism for the chemisorption process.

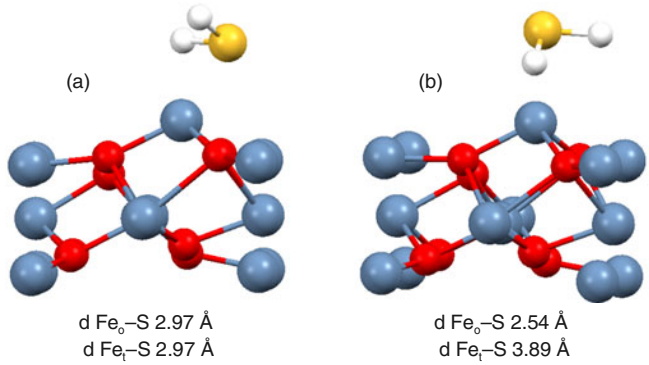

Fig. 14. Approximations of H_2S on Fe_o; (a) before adsorption; (b) after adsorption

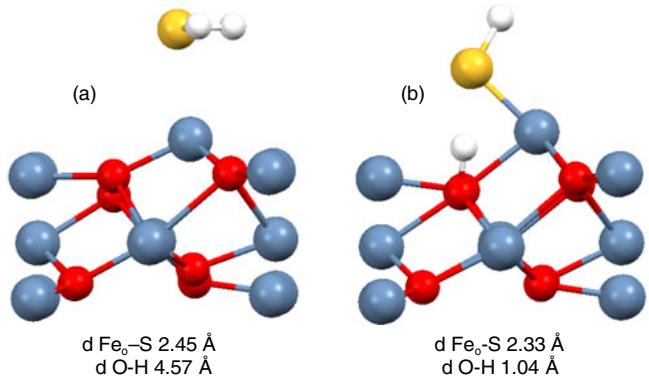

Fig. 15. Co-ordinate reaction of H_2S on Fe_o in Fe_o-Fe_t surface

Load transfer analysis was performed; the adsorption of H_2S causes an electronic transfer of octahedral iron Fe1 to the S atom of 0.07 electrons. This charge density affects the hydrogen atom H17 and acquires an electropositive character that allows it to interact with oxygen O6 on the surface. Finally, the load of the whole system remains neutral, leaving the surface with hydroxyl species. Table-10 shows the charges and magnetic moments of the atoms involved in the adsorption process.

TABLE-10
MAGNETIC MOMENTS AND CHARGES BEFORE ADSORPTION, IN THE PHYSISORPTION AND AFTER THE REACTION

Atom	Surface and H_2S isolated		Phisisorption		Quimisorption	
	Charge (u.a)	Magnetic moment (μ_B)	Charge (u.a)	Magnetic moment (μ_B)	Charge (u.a)	Magnetic moment (μ_B)
Fe1	1.62	3.62	1.57	3.61	1.64	3.66
Fe2	1.91	–3.88	1.87	–3.86	1.95	–3.93
O3	–1.53	0.04	–1.50	0.07	–1.54	0.07
O4	–1.53	0.04	–1.51	0.07	–1.53	0.06
O5	–1.53	0.04	–1.52	0.03	–1.55	0.08
O6	–1.23	0.55	–1.23	0.54	–1.02	0.20
Fe7	2.07	4.21	2.08	4.23	2.09	4.22
Fe8	2.07	4.21	2.04	4.19	2.10	4.24
Fe9	2.07	4.21	2.08	4.23	2.16	4.24
O10	–1.44	0.45	–1.42	0.46	–1.30	0.54
O11	–1.43	0.12	–1.44	0.08	–1.46	0.10
O12	–1.43	0.12	–1.43	0.10	–1.44	0.11
O13	–1.43	0.12	–1.43	0.10	–1.41	0.12
Fe14	1.82	–3.84	1.84	–3.86	1.84	–3.86
S15	–0.18	0.00	–0.26	0.03	–0.86	0.12
H16	0.09	0.00	0.11	0.00	0.13	0.01
H17	0.09	0.00	0.13	–0.01	0.25	0.01

Finally, the formation of links is related to the change in the density of states projected on the orbitals *d* of the iron octahedral Fe1 and the oxygen atom O6. Fig. 16 shows the DOS for Fe1, where the loss of the virtual *d* orbitals (clean surface) can be appreciated when the chemisorption process occurs, an overlap of the *d* orbitals of the iron with the *p* orbitals of the sulfur, while that the *p* orbitals of oxygen atom O6 move at lower energies when forming the bond between the atoms of O6-H17 (Fig. 17).

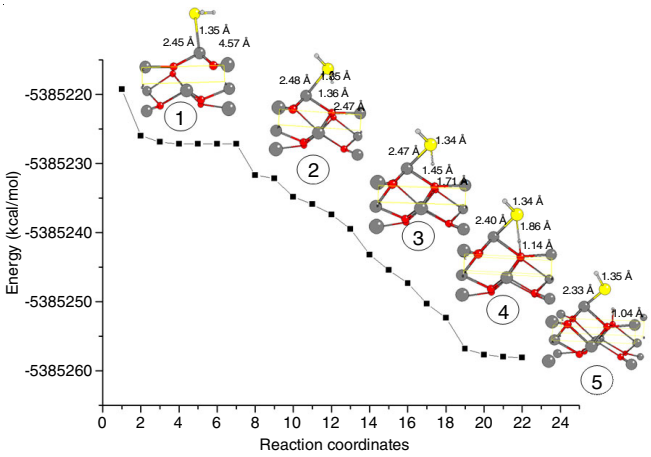

Fig. 16. Comparison of the projected DOS on the orbitals *d* of the iron octahedral Fe1 in the clean surface (dotted line) and after the adsorption (solid line)

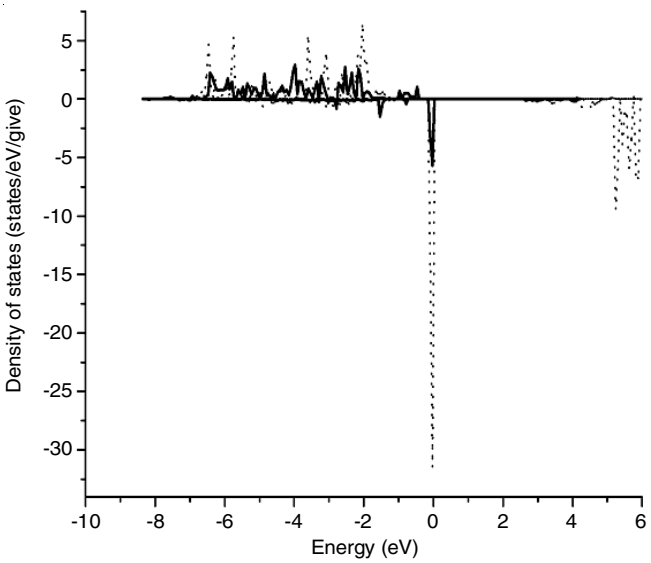

Fig. 17. Comparison of the DOS projected on the *p* orbitals of oxygen O6 on the clean surface (dotted line) and after the adsorption (solid line)

In 1st step a physisorption occurs, the H_2S molecule approaches the magnetite surface at a distance of 2.45 Å between the S atom with the Fe1 atom, the distance between H17 and O6 is 4.57 Å and the angle formed by the S-Fe1-O4 atoms was 122.6°. In 2nd step a reordering of the H_2S molecule occurs on the surface, the distance between the S-Fe atoms was 2.48 Å, the distance between the H17 and the O6 atom decreases considerably at 2.47 Å, the angle between the atoms S-Fe1-O4 is modified at 17.5° and the distance S-H17 increases from 1.35 to 1.36 Å.

In 3rd step the interactions of Fe1-S and O6-H17 are presented, where a distance between Fe1-S of 2.47 Å, a decrease of the distance O6-H17 to 1.71 Å and the distance S-H17 increases to 1.45 Å is observed. In the 4th step there is a rearrangement, break of the link S-H17 and bond formation O6-H17 at a distance of 1.14 Å and the distance S-Fe1 decreases to 2.40 Å. Finally, in the 5th step the system reaches a thermodynamically stable state, with link distances of 2.33 Å and 1.04 Å for Fe1-S and O6-H17, respectively.

The results obtained are similar to the water adsorption calculations on Fe_3O_4 (111) with Fe_o-Fe_t termination [38], where it is confirmed that the hydroxylated surface is favoured, the OH bond formation is thermodynamically stable and the dissociation energy of the mechanism is -26 kcal/mol.

The reaction mechanism between H_2S and the Fe_o-Fe_t surface is described according to the theoretical results: in the first step, the molecular adsorption of H_2S, later a rearrangement of the H_2S molecule and finally the breaking of the SH bond and formation of the H_2S molecule. OH bond on the surface, the SH group being linked to octahedral iron.

This step is based on [39], who proposed a similar mechanism for α-hematite (α-Fe_2O_3), an oxide with a termination similar to magnetite [19]. Davydov *et al.* [40] suggested that when H_2S and hematite come into contact with each other, a heterologous dissociation of H_2S and exchange of S^{2-} and HS^- by O^{2-} or HO^- is carried out, sulfur is oxidized to elemental S and Fe^{3+} cations reduced to Fe^{2+} and suggest the formation of HS^- anions on the surface as very reactive intermediates. In Fig. 18, this mechanism can be seen starting with the formation of O-H bonds on the surface, later the physisorption of other H_2S molecules occurs and then the formation of layers of iron and water sulphides occurs.

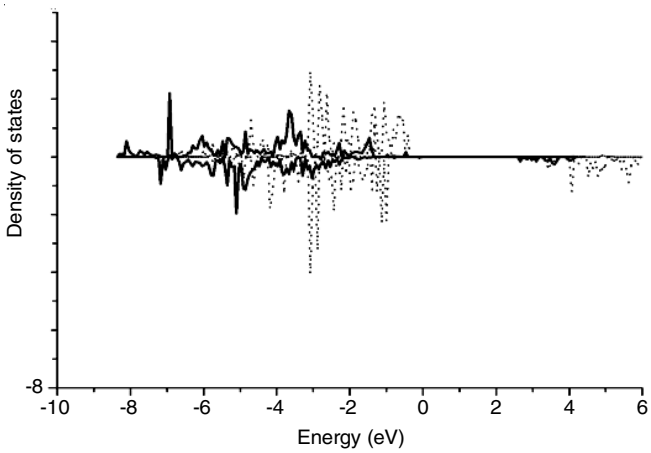

Fig. 18. Mechanism proposed for the interaction between α-Fe_2O_3 and H_2S molecule; Source: [Ref. 40]

Conclusion

The XRD patterns of Mn ferrites obtained show a majority phase corresponding to magnetite. The adsorption capacity of H_2S on the Mn ferrites indicates that the adsorption depends on the amount of iron and the temperature. The XRD patterns of the ferrites after H_2S adsorption show two crystalline phases corresponding to Fe_3O_4 and orthorhombic FeS_2 (marcasite). Calculations were made of the volume of magnetite, surfaces

and adsorption of H_2S on Fe_3O_4 (111) in the Fe_o-Fe_t termination with the code CRYSTAL09 using the functional PBE0 and the available bases of the program. An iron base was modified that improves volume, surface and adsorption results in magnetite for H_2S. The results of the BSSE in the calculation of the bridging H_2S adsorption energy were -17.50 kcal/mol when using the Fe(III) base, -12.51 kcal/mol using the Fe(III) and Fe(II) bases simultaneously and -4.99 kcal/mol with the modified base. The energy of the chemisorption process on octahedral iron was -48.42 kcal/mol, where the breakdown of the S-H bond in the H_2S molecule occurs and the formation of the O-H bond on the surface. This reaction mechanism is similar to that reported for the water molecule on the Fe_o-Fe_t surface of magnetite. The experimental and theoretical data indicate that the adsorption capacity of ferrites is limited to 50 %, since magnetite is the majority phase and it has two energetically favoured Fe_o-Fe_t and Fe_t-O terminations. However, the first one is the one that reacts with hydrogen sulfide.

ACKNOWLEDGEMENTS

The first author thanks the support to the National Council of Science and Technology (CONACYT) for the scholarship granted to study the Ph.D. in Chemistry within the doctorate program of the Autonomous University of the State of Hidalgo, included in the list of Postgraduate Programs of Excellence.

CONFLICT OF INTEREST

The authors declare that there is no conflict of interests regarding the publication of this article.

REFERENCES

1. H. Pinjing, S. Liming, Y. Zhiwen and L. Guojian, *Water Sci. Technol.*, **44**, 327 (2001); https://doi.org/10.2166/wst.2001.0564.
2. Y.N. Zhuravlev and O.S. Obolonskaya, *J. Struct. Chem.*, **51**, 1005 (2010); https://doi.org/10.1007/s10947-010-0157-1.
3. A. Dabrowski, Adsorption and Its Applications in Industry and Environmental Protection, Elsevier science B.V.: Holland, edn 1, vol. 1 (1999).
4. H.J. Glynn and G.W. Heinke, Ingeniería Ambiental, Prentice Hall: México, edn 2, pp. 537-540 (1999).
5. H. Pérez and P. Villa, *Agua Latinoamérica*, **3**, 17 (2005).
6. P.R. Westmoreland and D.P. Harrison, *Environ. Sci. Technol.*, **10**, 659 (1976); https://doi.org/10.1021/es60118a010.
7. T.J. Bandosz, A. Bagreev, F. Adib and A. Turk, *Environ. Sci. Technol.*, **34**, 1069 (2000); https://doi.org/10.1021/es9813212.
8. H.L. Chiang, J.H. Tsai, H.L. Tsai and Y.C. Hsu, *Sep. Sci. Technol.*, **35**, 903 (2000); https://doi.org/10.1081/SS-100100200.
9. Y.N. Zhuravlev and O.S. Obolonskaya, *Russ. Phys. J.*, **53**, 776 (2011); https://doi.org/10.1007/s11182-011-9489-3.
10. L. Mino, A.M. Ferrari, V. Lacivita, G. Spoto, S. Bordiga and A. Zecchina, *J. Phys. Chem. C*, **115**, 7694 (2011); https://doi.org/10.1021/jp2017049.
11. A.S. Mazheika, T. Bredow, V.E. Matulis and O.A. Ivashkevich, *J. Phys. Chem. C*, **115**, 17368 (2011); https://doi.org/10.1021/jp200575u.
12. C.-T. Yang, N. Balakrishnan, V.R. Bhethanabotla and B. Joseph, *J. Phys. Chem. C*, **118**, 4702 (2014); https://doi.org/10.1021/jp4112525.
13. V.E. Alexandrov, E.A. Kotomin, J. Maier and R.A. Evarestov, *Eur. Phys. J. B*, **72**, 53 (2009); https://doi.org/10.1140/epjb/e2009-00339-4.
14. R.A.P. Ribeiro, A. Camilo Jr. and S.R. de Lazaro, *J. Magn. Magn. Mater.*, **394**, 463 (2015); https://doi.org/10.1016/j.jmmm.2015.05.096.
15. J. Kim, A.J. Ilott, D.S. Middlemiss, N.A. Chernova, N. Pinney, D. Morgan and C.P. Grey, *Chem. Mater.*, **27**, 3966 (2015); https://doi.org/10.1021/acs.chemmater.5b00856.
16. J. Navarro-Ruiz, P. Ugliengo, A. Rimola and M. Sodupe, *J. Phys. Chem. A*, **118**, 5866 (2014); https://doi.org/10.1021/jp4118198.
17. J. Ahdjoudj, C. Martinsky, C. Minot, M.A. Van Hove and G.A. Somorjai, *Surf. Sci.*, **443**, 133 (1999); https://doi.org/10.1016/S0039-6028(99)01008-0.
18. A.D. Rowan, C.H. Patterson and L.V. Gasparov, *Phys. Rev. B*, **79**, 205103 (2009); https://doi.org/10.1103/PhysRevB.79.205103.
19. C.H. Patterson, *Phys. Rev. B*, **90**, 075134 (2014); https://doi.org/10.1103/PhysRevB.90.075134.
20. N.G. Condon, P.W. Murray, F.M. Leibsle, G. Thornton, A.R. Lennie and D.J. Vaughan, *Surf. Sci.*, **310**, L609 (1994); https://doi.org/10.1016/0039-6028(94)91360-9.
21. M.E. Grillo, M.W. Finnis and W. Ranke, *Phys. Rev. B*, **77**, 075407 (2008); https://doi.org/10.1103/PhysRevB.77.075407.
22. E. Aquino, F. Prieto, C.A. Galán, C.A. González, E. Barrado and J. Medina, *Revista Dyna*, **78**, 78 (2011).
23. G. B arrera, F. Prieto, M.A. Méndez, A.M. Bolarín and F. Sánchez, *Rev. Lat. Amer. Met. Mat. Venezuela*, **27**, 95 (2007).
24. C. Pisani, R. Dovesi and C. Roetti, Hartree-Fock *ab-initio* Treatment of Crystalline Systems: In Lecture Notes in Chemistry, Springer: Berlin/Heidelberg/New York, vol. 48, p. 193 (1988).
25. E. Aquino and F. Prieto, ed.: J. Cruz, Absorción de sulfuro de hidrogeno sobre ferritas. Un estudio teórico-experimental. Editorial Académica Española, p. 42 (2012).
26. F. Labat, P. Baranek and C. Adamo, *J. Chem. Theory Comput.*, **4**, 341 (2008); https://doi.org/10.1021/ct700221w.
27. M. Catti, G. Valerio and R. Dovesi, *Phys. Rev. B*, **51**, 7441 (1995); https://doi.org/10.1103/PhysRevB.51.7441.
28. G. Valerio, M. Catti, R. Dovesi and R. Orlando, *Phys. Rev. B*, **52**, 2422 (1995); https://doi.org/10.1103/PhysRevB.52.2422.
29. R. Krishnan, J.S. Binkley, R. Seeger and J.A. Pople, *J. Chem. Phys.*, **72**, 650 (1980); https://doi.org/10.1063/1.438955.
30. M.D. Towler, N.L. Allan, N.M. Harrison, V.R. Saunders, W.C. Mackrodt and E. Apra, *Phys. Rev. B*, **50**, 5041 (1994); https://doi.org/10.1103/PhysRevB.50.5041.
31. N.-O. Ikenaga, Y. Ohgaito and T. Suzuki, *Energy Fuels*, **19**, 170 (2005); https://doi.org/10.1021/ef049907z.
32. A. Barbieri, W. Weiss, M.A. Van Hove and G.A. Somorjai, *Surf. Sci.*, **302**, 259 (1994); https://doi.org/10.1016/0039-6028(94)90832-X.
33. E.J. Nejat, A.J. Polotsky and L. Pal, *Maturitas*, **65**, 106 (2010); https://doi.org/10.1016/j.maturitas.2009.09.006.
34. W. Weiss and W. Ranke, *Prog. Surf. Sci.*, **70**, 1 (2002); https://doi.org/10.1016/S0079-6816(01)00056-9.
35. R. Aragón, *Phys. Rev. B*, **46**, 5328 (1992); https://doi.org/10.1103/PhysRevB.46.5328.
36. J.P. Wright, J.P. Attfield and P.G. Radaelli, *Phys. Rev. B*, **66**, 214422 (2002); https://doi.org/10.1103/PhysRevB.66.214422.
37. R.E. Hummel, Electronic Properties of Materials, Springer: Nueva York, edn 4, pp. 68-70 (2011).
38. A.R. Lennie, N.G. Condon, F.M. Leibsle, P.W. Murray, G. Thornton and D.J. Vaughan, *Phys. Rev. B*, **53**, 10244 (1996); https://doi.org/10.1103/PhysRevB.53.10244.
39. C. Zhou, Q. Zhang, L. Chen, B. Han, G. Ni, J. Wu, D. Garg and H. Cheng, *J. Phys. Chem. C*, **114**, 21405 (2010); https://doi.org/10.1021/jp105040v.
40. A. Davydov, K.T. Chuang and A.R. Sanger, *J. Phys. Chem. B*, **102**, 4745 (1998); https://doi.org/10.1021/jp980361p.